ACCOUNTS
of chemical research

Molecular Dynamics Simulation of Nonlinear Spectroscopies of Intermolecular Motions in Liquid Water

TAKUMA YAGASAKI[†] AND SHINJI SAITO[*,†,‡]

[†]*Department of Theoretical and Computational Molecular Science, Institute for Molecular Science, Myodaiji, Okazaki, Aichi, 444-8585, Japan,* [‡]*The Graduate University for Advanced Studies, Myodaiji, Okazaki, Aichi, 444-8585, Japan*

RECEIVED ON JANUARY 6, 2009

CONSPECTUS

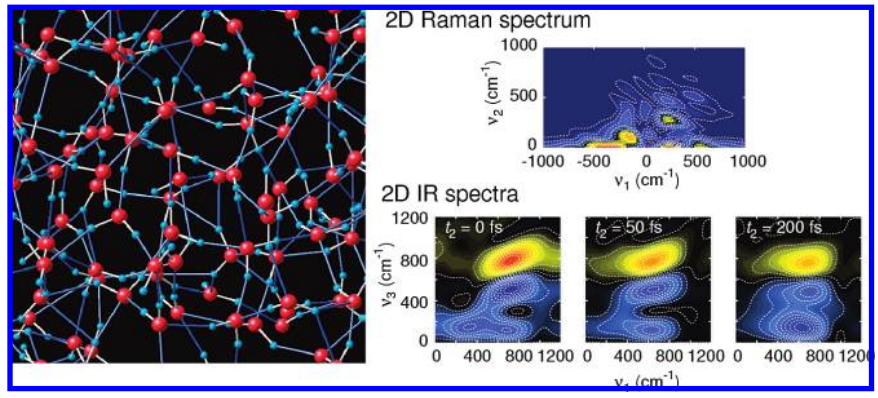

Water is the most extensively studied of liquids because of both its ubiquity and its anomalous thermodynamic and dynamic properties. The properties of water are dominated by hydrogen bonds and hydrogen bond network rearrangements. Fundamental information on the dynamics of liquid water has been provided by linear infrared (IR), Raman, and neutron-scattering experiments; molecular dynamics simulations have also provided insights.

Recently developed higher-order nonlinear spectroscopies open new windows into the study of the hydrogen bond dynamics of liquid water. For example, the vibrational lifetimes of stretches and a bend, intramolecular features of water dynamics, can be accurately measured and are found to be on the femtosecond time scale at room temperature. Higher-order nonlinear spectroscopy is expressed by a multitime correlation function, whereas traditional linear spectroscopy is given by a one-time correlation function. Thus, nonlinear spectroscopy yields more detailed information on the dynamics of condensed media than linear spectroscopy.

In this Account, we describe the theoretical background and methods for calculating higher order nonlinear spectroscopy; equilibrium and nonequilibrium molecular dynamics simulations, and a combination of both, are used. We also present the intermolecular dynamics of liquid water revealed by fifth-order two-dimensional (2D) Raman spectroscopy and third-order IR spectroscopy. 2D Raman spectroscopy is sensitive to couplings between modes; the calculated 2D Raman signal of liquid water shows large anharmonicity in the translational motion and strong coupling between the translational and librational motions. Third-order IR spectroscopy makes it possible to examine the time-dependent couplings. The 2D IR spectra and three-pulse photon echo peak shift show the fast frequency modulation of the librational motion. A significant effect of the translational motion on the fast frequency modulation of the librational motion is elucidated by introducing the "translation-free" molecular dynamics simulation. The isotropic pump-probe signal and the polarization anisotropy decay show fast transfer of the librational energy to the surrounding water molecules, followed by relaxation to the hot ground state. These theoretical methods do not require frequently used assumptions and can thus be called *ab initio* methods; together with multidimensional nonlinear spectroscopies, they provide powerful methods for examining the inter- and intramolecular details of water dynamics.

Published on the Web 05/26/2009 www.pubs.acs.org/acr
10.1021/ar900007s CCC: $71.50

I. Introduction

Water is one of the most ubiquitous substances on earth and one of the most puzzling substances in chemistry and physics. In ice Ih, water molecules make four hydrogen bonds (HBs) with surrounding molecules and expand the three-dimensional HB network. Since only 10% of HBs are broken by melting, the three-dimensional HB network, though highly distorted, remains in the liquid phase. The HB network yields a number of anomalous properties, e.g., large heat capacity, high melting and boiling temperatures and density maximum at 4 °C.[1,2] It is well-known that various chemical processes in water are dominated by HB dynamics such as the forming and breaking of HBs and the resulting HB network rearrangements.[3−11]

Nonlinear spectroscopy can yield detailed information on dynamics which is not evident from linear spectroscopy. Recent third-order IR spectroscopic experiments have provided a wealth of information on the dynamics of liquid water. Pump−probe experiments have shown that the vibrational lifetime of the OH stretch in pure water is 200−260 fs and that of the HOH bend is 170−260 fs.[12−19] The polarization anisotropy of the OH stretch in pure water decays with a time scale of 80 fs.[13,14,20] Two-dimensional (2D) IR spectroscopy has revealed that the spectral diffusion of the OH stretch occurs on a sub-50 fs time scale at 300 K.[13,14] The OH stretch of HOD in D_2O and the OD stretch of HOD in H_2O have been also extensively investigated by various nonlinear spectroscopic techniques.[20−28] In addition to these experimental studies, theoretical studies have provided much insight into the dynamics of the hydroxyl stretch of water.[29−36]

Besides knowledge of the intramolecular motions, that of intermolecular motions is also essential for the elucidation of the HB dynamics of water. Chieffo et al. performed the pump−probe experiment of pure water in which the bend−libration combination band, 2130 cm^{-1}, is excited.[19] Ashihara et al. measured the pump−probe signal by using the pump pulse centered at 1350 cm^{-1} which excites the high-frequency librational band and/or the libration combination band.[37] However, there have been no third-order IR spectroscopic experiments in which intermolecular motions below 1000 cm^{-1} are directly excited.

Fifth-order 2D Raman spectroscopy is a powerful nonlinear spectroscopic technique to investigate the intermolecular dynamics of hydrogen bonded liquids.[38−43] Very recently, Miller et al. have succeeded in the 2D Raman experiment of liquid formamide.[40] However, it is still impossible to experimentally measure the 2D Raman signal of liquid water because of the small anisotropic polarizability of water.

It is difficult to theoretically investigate the intermolecular dynamics in terms of nonlinear spectroscopy. The intermolecular motions are collective.[5,6,44] In addition, the intermolecular motions change their natures and frequencies in a complicated manner with the rearrangement of the liquid structure. Therefore, the conventional methods used for the intramolecular motions cannot be applied to the calculation of the nonlinear response function of the intermolecular motions.

Great progress has been achieved in developing theoretical methods for nonlinear spectroscopy of the intermolecular motions.[41−43,45−55] Recently, computational methods for nonlinear spectroscopy by using classical equilibrium and/or nonequilibrium molecular dynamics (MD) simulations have been developed and applied to several systems.[41−43,45,46,51−55] Once the dipole moment or the polarizability is calculated along a trajectory, these methods make it possible to evaluate the nonlinear response function of the intermolecular motions as well as the intramolecular motions. Furthermore, these methods do not need frequently used assumptions, i.e., the second-order cumulant expansion and the Condon approximation. Thus, these methods can be called *ab initio* methods for the calculation of nonlinear spectroscopy.

In this Account, we introduce *ab initio* methods for the nonlinear response functions. Then, we review our recent progress in the study of the intermolecular dynamics of liquid water by using various nonlinear spectroscopic techniques.

II. Computational Methodology

We describe the computational methodology for fifth-order Raman and third-order IR response functions. The derivations in this section are easily applied to nonlinear IR and Raman response functions of arbitrary order.

Fifth-Order Raman Response Function. The system is initially in an equilibrium state expressed by the density matrix $\rho_{eq} = \exp(-\beta H_0)/Z$, where β, H_0, and Z are the reciprocal temperature, the system Hamiltonian and the partition function, respectively. The fifth-order 2D Raman response function is given by[38,39,56,57]

$$S^{(5)}_{\mathrm{Raman}}(t_1, t_2) = \left(\frac{\mathrm{i}}{\hbar}\right)^2 tr\{\Pi(t_1 + t_2)[\Pi(t_1), [\Pi(0), \rho_{eq}]]\} \quad (1)$$

where $\Pi(t)$ is the polarizability operator of the system at t. Equation 1 can be recast as

$$S^{(5)}_{\text{Raman}}(t_1, t_2) = \beta \frac{\mathrm{i}}{\hbar} \langle \widetilde{\dot{\Pi}}(0)[\Pi(t_1 + t_2), \Pi(t_1)] \rangle \quad (2)$$

where $\widetilde{\dot{\Pi}}(0)$ is the Kubo transform of $\dot{\Pi}(0)$. The corresponding classical response function is given by

$$S^{(5)}_{\text{Raman}}(t_1, t_2) = -\beta \langle \dot{\Pi}(0)\{\Pi(t_1 + t_2), \Pi(t_1)\}_{\text{PB}} \rangle \quad (3)$$

where $\{\ ,\ \}_{\text{PB}}$ is the Poisson bracket. Equation 3 is called the equilibrium dynamics method because it can be evaluated from the equilibrium MD simulation.[41,45]

When we introduce the following relation[58]

$$\frac{i}{\hbar}[\Pi,\ ] = \lim_{\varepsilon \to 0} \frac{1}{\varepsilon} \left\{ \exp\left(\frac{i}{\hbar} \varepsilon [\Pi,\ ] \right) - 1 \right\} \quad (4)$$

we can rewrite eq 2 as

$$S^{(5)}_{\text{Raman}}(t_1, t_2) = \lim_{\varepsilon \to 0} \frac{\beta}{\varepsilon} \langle \widetilde{\dot{\Pi}}(0)(\Pi_{t_1}(t_1 + t_2) - \Pi(t_1 + t_2)) \rangle \quad (5)$$

with

$$\Pi_{t_1}(t_1 + t_2) = \exp\left\{ \frac{\mathrm{i}}{\hbar} \int_0^{t_1 + t_2} (H_0 - \delta(t_1)\varepsilon\Pi)\, \mathrm{d}t \right\} \times \Pi \exp\left\{ -\frac{\mathrm{i}}{\hbar} \int_0^{t_1 + t_2} (H_0 - \delta(t_1)\varepsilon\Pi)\, \mathrm{d}t \right\} \quad (6)$$

where ε is a perturbation parameter and $\delta(t)$ is the delta function. By using the inverted force method,[59] we have

$$S^{(5)}_{\text{Raman}}(t_1, t_2) = \lim_{\varepsilon \to 0} \frac{\beta}{2\varepsilon} \langle \widetilde{\dot{\Pi}}(0)(\Pi_{t_1}(t_1 + t_2) - \Pi_{\bar{t}_1}(t_1 + t_2)) \rangle \quad (7)$$

where the overbar on the subscript of the second term indicates the oppositely polarized electric field. The corresponding classical expression is given by[51,53]

$$S^{(5)}_{\text{Raman}}(t_1, t_2) = \lim_{\varepsilon \to 0} \frac{\beta}{2\varepsilon} \langle \dot{\Pi}(0)(\Pi_{t_1}(t_1 + t_2) - \Pi_{\bar{t}_1}(t_1 + t_2)) \rangle \quad (8)$$

Since $\Pi_{t_1}(t_1 + t_2)$ and $\Pi_{\bar{t}_1}(t_1 + t_2)$ are calculated from the nonequilibrium MD simulations in which an electric field is applied at t_1, this method is called the nonequilibrium dynamics method. Equation 8 shows that the 2D Raman response function is calculated as the product of the time derivative of the polarizability at $t = 0$ and the difference in the polarizabilities at $t_1 + t_2$ on the two perturbed trajectories.

Third-Order IR Response Function. The third-order IR response function is given by[39,56,57]

$$S^{(3)}_{\text{IR}}(t_1, t_2, t_3) = \left(\frac{i}{\hbar} \right)^3 tr\{M(t_1 + t_2 + t_3)[M(t_1 + t_2), [M(t_1), [M(0), \rho_{\text{eq}}]]]\} \quad (9)$$

where $M(t)$ is the dipole moment operator of the system at t. By shifting time by t_1 and using the operation given by eq 4, we have[55]

$$S^{(3)}_{\text{IR}}(t_1, t_2, t_3) = \lim_{\varepsilon \to 0} \frac{\beta}{4\varepsilon^2} (\langle \widetilde{\dot{M}}(-t_1) M_{\bar{t}_2,\bar{0}}(t_2 + t_3) \rangle - \langle \widetilde{\dot{M}}(-t_1) M_{\bar{t}_2,0}(t_2 + t_3) \rangle - \langle \widetilde{\dot{M}}(-t_1) M_{t_2,\bar{0}}(t_2 + t_3) \rangle + \langle \widetilde{\dot{M}}(-t_1) M_{t_2,0}(t_2 + t_3) \rangle) \quad (10)$$

where we employed the inverted force method and $M_{t_2,0}(t_2 + t_3)$ is the dipole moment at $t_2 + t_3$ in the presence of the external fields at $t = 0$ and t_2.

Equation 9 can be reexpressed as

$$S^{(3)}_{\text{IR}}(t_1, t_2, t_3) = \beta \left(\frac{i}{\hbar} \right)^2 tr\{[M(t_2 + t_3), M(t_2)][M(0), \rho_{\text{eq}} \widetilde{\dot{M}}(-t_1)]\} = \beta \left\langle \left(\beta \widetilde{\dot{M}}(0)\, \widetilde{\dot{M}}(-t_1) + \frac{i}{\hbar} [M(0), \widetilde{\dot{M}}(-t_1)] \right) \frac{i}{\hbar} [M(t_2 + t_3), M(t_2)] \right\rangle \quad (11)$$

By using eq 4 and the inverted force method, we have[54]

$$S^{(3)}_{\text{IR}}(t_1, t_2, t_3) = \langle D(0; -t_1)\, W(t_3; t_2) \rangle - \langle D(0; -t_1) \rangle \langle W(t_3; t_2) \rangle \quad (12)$$

with

$$D(0; -t_1) = \beta^2 \widetilde{\dot{M}}(0)\, \widetilde{\dot{M}}(-t_1) + \lim_{\varepsilon \to 0} \frac{\beta}{2\varepsilon} \left(\widetilde{\dot{M}}_0(-t_1) - \widetilde{\dot{M}}_{\bar{0}}(-t_1) \right) \quad (13)$$

$$W(t_3; t_2) = \lim_{\varepsilon \to 0} \frac{1}{2\varepsilon} (M_{t_2}(t_2 + t_3) - M_{\bar{t}_2}(t_2 + t_3)) \quad (14)$$

The classical third-order response functions corresponding to eqs 10 and 12 are obtained by substituting $\widetilde{\dot{M}}$ with $\dot{M}$. All terms in eq 10 are calculated from the nonequilibrium MD simulations in which two electric field pulses are explicitly applied at 0 and t_2. The function $W(t_3;t_2)$ is calculated from two forward nonequilibrium MD simulations in which an electric field pulse is applied at t_2 and the second term of $D(0;\text{-}t_1)$ is calculated from two backward nonequilibrium MD simulations in which an electric field pulse is applied at $t = 0$. The calculation of eq 12 is more efficient than that of eq 10 because the equilibrium trajectory is used for the t_2 period.[54]

There are four possible phase matching directions in third-order IR spectroscopy, i.e. $\mathbf{k}_{\text{I}} = -\mathbf{k}_1 + \mathbf{k}_2 + \mathbf{k}_3$, $\mathbf{k}_{\text{II}} = \mathbf{k}_1 - \mathbf{k}_2 + \mathbf{k}_3$, $\mathbf{k}_{\text{III}} = \mathbf{k}_1 + \mathbf{k}_2 - \mathbf{k}_3$ and $\mathbf{k}_{\text{IV}} = \mathbf{k}_1 + \mathbf{k}_2 + \mathbf{k}_3$ where $\mathbf{k}_1$, $\mathbf{k}_2$ and $\mathbf{k}_3$ are the wave vectors of three incident electric fields. The calculated third-order response function contains the nonlinear responses of all the four directions. The 2D IR correlation spectrum is defined as the sum of signals of the directions $\mathbf{k}_{\text{I}}$ and $\mathbf{k}_{\text{II}}$.[60,61] Therefore, the nonlinear responses of the direc-

tions $\mathbf{k}_{III}$ and $\mathbf{k}_{IV}$ have to be removed from the calculated response function.

The signals of the directions $\mathbf{k}_{III}$ and $\mathbf{k}_{IV}$ show highly oscillatory behavior during the waiting time t_2, and thus they can be separated from the calculated third-order response function by using the 3D Fourier transform[54,55]

$$S^{(3)}_{IR}(\nu_1, \nu_2, \nu_3) = \int_0^\infty dt_3 \int_0^\infty dt_2 \int_0^\infty dt_1\, S^{(3)}_{IR}(t_1, t_2, t_3)\, e^{2\pi c i(\nu_1 t_1 + \nu_2 t_2 + \nu_3 t_3)} \quad (15)$$

Alternatively, we can obtain the signal corresponding to a specific phase matching condition by directory evaluating the convolution of the third-order response function with the electric fields

$$P^{(3)}(\tau, T, t) = \int_0^\infty dt_3 \int_0^\infty dt_2 \int_0^\infty dt_1\, E(t_s - t_3) \times E(t_s - t_3 - t_2)\, E(t_s - t_3 - t_2 - t_1)\, S^{(3)}_{IR}(t_1, t_2, t_3) \quad (16)$$

with

$$E(t) = \sum_{j=1}^{3} \varepsilon_j(t)\, e^{-i\omega j t}\, e^{i\mathbf{k}_j \cdot \mathbf{r}} + \varepsilon_j^*(t)\, e^{i\omega j t}\, e^{-i\mathbf{k}_j \cdot \mathbf{r}} \quad (17)$$

where three time intervals are defined as $\tau = \tau_2 - \tau_1$, $T = \tau_3 - \tau_2$ and $t = t_s - \tau_3$ with the pulse center times τ_1, τ_2, and τ_3. $\varepsilon_j(t)$, ω_j and $\mathbf{k}_j$ denote the pulse envelope, the carrier frequency and the wave vector of the jth pulse, respectively. Equation 16 can be decomposed into eight terms corresponding to the four phase matching components and their complex conjugates. We can obtain the 2D IR correlation spectrum by taking the 2D Fourier transform of the polarizations of $\mathbf{k}_I$ and $\mathbf{k}_{II}$ with respect to τ and t.

III. Intermolecular Dynamics of Liquid Water

Figure 1 shows the intermolecular density of states of liquid water calculated from

$$f(\nu) = \frac{\beta}{3\pi} \int_{-\infty}^{\infty} dt\, e^{2\pi c i \nu t} \sum_i m_i \langle v_i(t)\, v_i(0) \rangle \quad (18)$$

where m_i and v_i are the mass and velocity of atom i, respectively. Unlike most liquids such as CH_3CN and CS_2, liquid water shows the dynamics over a wide range of frequencies from 0 to 1000 cm^{-1}. The density of states below 300 cm^{-1} is attributed to the translational motion. The translational motion has a peak at 50 cm^{-1} and a shoulder at 200 cm^{-1}. These are assigned to the O−O−O HB bend and the O−O HB stretch, respectively. The librational motion shows a broadband from

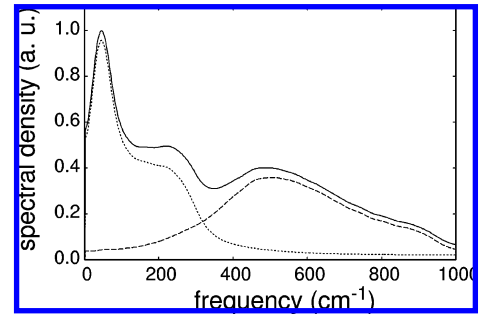

FIGURE 1. Intermolecular density of states of liquid water (solid line). The dotted and dashed lines are contributions from the translational and librational motions, respectively.

400 to 1000 cm^{-1}. These intermolecular modes are observed in the one-dimensional (1D) infrared, low frequency Raman, and neutron scattering experiments. The 1D spectroscopic methods provide fundamental information on dynamics, e.g., the peak position and the bandwidth. However, it is difficult to investigate the static and dynamic couplings between modes by using the 1D spectroscopic methods. Detailed information on the intermolecular dynamics of liquid water such as the mode couplings and the energy relaxation is revealed by multidimensional spectroscopy in the following sections.

IV. Intermolecular Dynamics of Liquid Water Analyzed Using Nonlinear Spectroscopy

A. Fifth-Order Raman Spectroscopy. Figure 2(a) shows the all-parallel polarization component of the fifth-order 2D Raman response of liquid water at 300 K and 1.0 g/mL. The flexible SPC potential is used. Other computational details are presented in ref 43. The 2D Raman signal shows the first positive peak at (t_1, t_2) = (∼35 fs, ∼15 fs), the second peak at (∼60 fs, ∼75 fs) and the weak tails from the second peak along the t_2 axis and the diagonal line of $t_1 = t_2$. It also shows the strong negative response near the t_2 axis. The first and second peaks mainly arise from the translational term and the cross term of the translational and librational motions. These terms also contribute to the tails from the second peak and

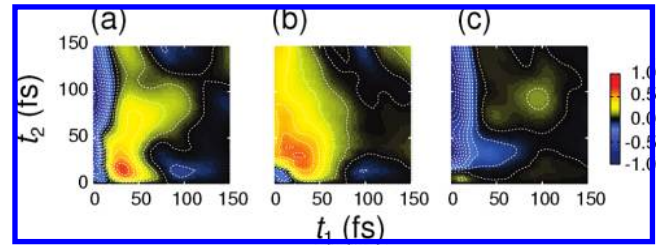

FIGURE 2. (a) All-parallel polarization component of 2D Raman response function of liquid water. (b) Nonlinear polarizability and (c) mechanical anharmonicity components of the 2D Raman response function.

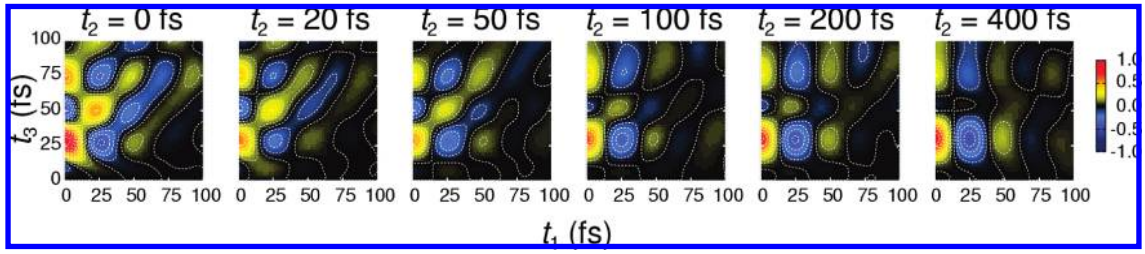

FIGURE 3. Third-order nonlinear IR response functions of liquid water at several waiting times.

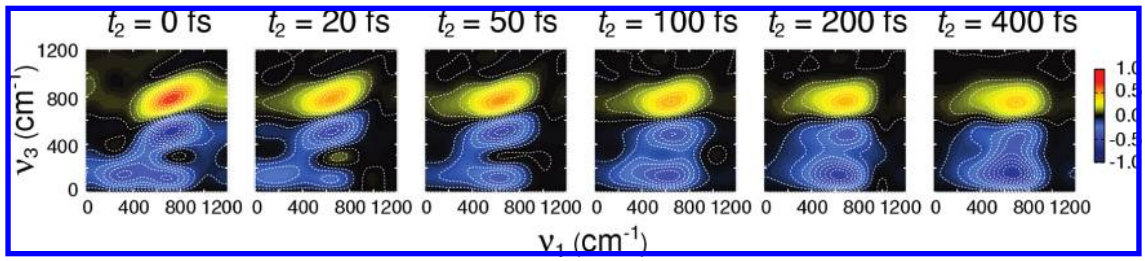

FIGURE 4. 2D IR correlation spectra of intermolecular motions in liquid water. Electric fields are assumed to be the delta function.

the negative response near the t_2 axis. The negative response at (∼15 fs, ∼15 fs) and the weak diagonal signal are attributed to the librational motion. The complicated 2D Raman signal results from the mode coupling between the translational and the librational motions.

2D Raman spectroscopy is sensitive to the nonlinear dynamics caused by the nonlinear polarizability and the mechanical anharmonicity.[51,62] Figure 2(b) shows the nonlinear polarizability component of the fifth-order response. The translational nonlinear polarizability yields the positive peak at (∼35 fs, ∼35 fs). The negative peak at (∼15 fs, ∼15 fs) and the tail along the t_2 axis result from the librational nonlinear polarizability. Figure 2(c) shows the fifth-order response arising from the mechanical anharmonicity. It shows the strong negative response near $t_1 = 0$ which is attributed to the translational motion and the cross term. This negative response decays quickly with the increase of t_1 because the anharmonic effect depends on the correlation between the stability matrix $\partial q(t_2 + t_1)/\partial p(t_1)$ and the velocity $p(0)/m$.

2D Raman spectroscopy reveals that the intermolecular translational motion in liquid water has the large anharmonicity. It is also shown that the large anharmonicity induces the strong coupling between the translational and librational motions as well as that between the translational motions. It should be noted that the mode couplings of the nonlinear polarizability and the mechanical anharmonicity are also clearly seen in the frequency domain, i.e. the 2D Raman spectrum.[43]

B. Third-Order IR Spectroscopy. As shown in the previous section, the mode coupling can be analyzed in detail by using 2D Raman spectroscopy with two time variables. Third-order IR spectroscopy with three time variables makes it possible to investigate the time dependent mode couplings and the energy relaxation. In this section, we show the third-order IR signals of intermolecular motions in liquid water. The SPC/E model is used for the water−water interaction potential. The details of simulation procedure are presented in ref 55.

Frequency Fluctuation. Figure 3 shows the third-order IR response functions of liquid water at 300 K and 1.0 g/mL.[55] The diagonally elongated signals are clearly seen at small t_2, because of the presence of the correlation between motions during t_1 and t_3. The diagonally elongated signal becomes weak with the increase of t_2 due to the frequency fluctuation. The diagonal signal almost disappears for $t_2 \geq 100$ fs, and the response function looks like the direct product of the correlation function along t_1 axis and the response function along t_3 axis.

The 2D IR correlation spectra at several t_2 are shown in Figure 4. The positive peak at $(\nu_1,\nu_3) = (\sim 750\ \text{cm}^{-1}, \sim 800\ \text{cm}^{-1})$ is due to the stimulated emission and the bleaching of the librational motion, whereas the negative peak at (∼720 cm^{-1}, ∼500 cm^{-1}) is due to the excited state absorption. These peaks are diagonally elongated at small waiting times because of the presence of the strong correlation between frequencies ν_1 and ν_3. The tilt angle between the nodal line of the diagonal librational peak and the ν_1 axis decreases with increasing t_2 due to the loss of frequency correlation.[63] Open circles in Figure 5 show the waiting time dependence of the tilt angle. The tilt angle decays monotonically and the time scale is approximately 115 fs when the decay is fitted with a single exponential function.

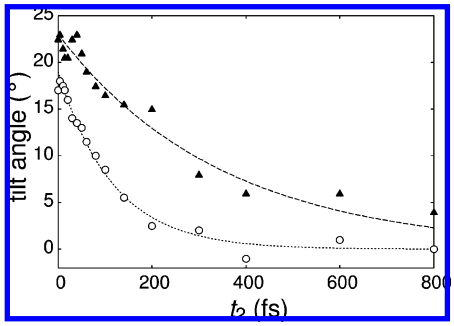

FIGURE 5. Waiting time dependence of the tilt angle. Open circles and solid triangles are the results in the presence and absence of the translational motion. The dotted and dashed lines are 19 $\exp(-t_2/115)$ and 23 $\exp(-t_2/367)$, respectively.

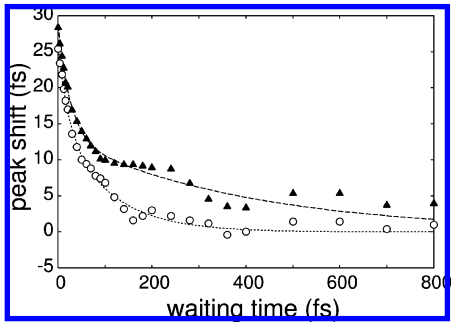

FIGURE 6. 3PEPS of the librational motion of liquid water. Photon echo signals are calculated from eq 16 with 60 fs pulses centered at 700 cm^{-1}. Open circles and solid triangles are the results in the presence and absence of the translational motion. The dotted and dashed lines are 10 $\exp(-T/21) + 16\exp(-T/103)$ and 15 $\exp(-T/26) + 13\exp(-T/394)$, respectively.

The three-pulse photon echo peak shift (3PEPS) is one of the most sensitive probes for the frequency fluctuation.[64] Figure 6 shows the 3PEPS of the librational motion of liquid water. The 3PEPS is well fit by the sum of two exponential functions with time scales of 21 and 103 fs, respectively. The time scale of the slower component is in good agreement with that of the tilt angle. The faster component, which is not seen in the tilt angle, is attributed to the fluctuation arising from the librational motion.

2D Raman spectroscopy revealed the strong coupling between the translational and librational motions in liquid water. In order to investigate the effect of the coupling on the 2D IR spectra, we calculated the third-order response functions by using the translation-free MD simulation.[55] The initial configuration for the translation-free MD simulation was taken from the trajectory in the presence of the translational motion. The translation-free MD trajectory was calculated by subtracting the force on center of masses at every time step and thus the HB network does not change in the simulation. The 2D IR correlation spectra calculated from the translation-free simulation are shown in Figure 7. The correlation spectrum at $t_2 = 0$ fs in the absence of the translational motion is similar to that in the presence of the translational motion (Figure 4). At large t_2, however, the difference between spectra in the presence and absence of the translational motion becomes significant; the librational peak is still tilted even for $t_2 > 200$ fs in the absence of the translational motion. The waiting time dependence of the tilt angle and the 3PEPS are presented by solid triangles in Figures 5 and 6. These figures clearly show that the loss of the frequency correlation of the librational motion significantly slows down in the absence of the translational motion. This result indicates that the anharmonicity induced by the translational motion, i.e., the O−O HB stretch and the O−O−O HB bend, results in the ultrafast loss of frequency correlation of the librational motion.

Energy Relaxation of Librational Motion. Understanding the energy relaxation in liquid water is quite important because it is involved in various chemical processes.[65,66] Lock and Bakker showed that the OH stretch excitation relaxes to the overtone of the HOH bending mode.[12] The subsequent studies with the two color pump−probe signal showed that the librational motion is also an important intermediate state in the energy cascading process in liquid water.[15−19,37] It is well established that the energy relaxation of the intramolecular motions leads the system into the "hot ground state".[12,13,15−19,37] The hot ground state has different optical properties from the initial ground state, because HBs are weakened in the hot ground state due to the "thermalization". The studies with ultrafast IR nonlinear spectroscopy revealed the detailed mechanism of the energy relaxation of the intramolecular motions. However, little is known about the energy cascading process of the low frequency intermolecular motions. We demonstrate that theoretical nonlinear spectroscopy can elucidate the energy cascading process of the low frequency motions in liquid water.

The 2D IR spectra show the distinct off-diagonal peak at $(\nu_1,\nu_3) = (\sim 700\ cm^{-1}, \sim 150\ cm^{-1})$ (Figure 4). The waiting time dependence of the off-diagonal peak shows the detailed relaxation dynamics of the librational motion. The intensity change of the negative off-diagonal peak is decomposed into three components, i.e. the decrease of the oscillatory behavior for $t_2 < 50$ fs, the fast increase for $t_2 < 100$ fs and the slow increase. The decrease of the oscillatory behavior at the off-diagonal peak shows the relaxation of the coherent state created by the excitations with different frequencies at $t = 0$ and t_1 (Figure 8(a)). The fast increase for $t_2 < 100$ fs can be attributed to the energy relaxation from the librational motion to the low frequency motion. An example of the diagrams corresponding to this relaxation is shown in Figure 8(b). The slow-

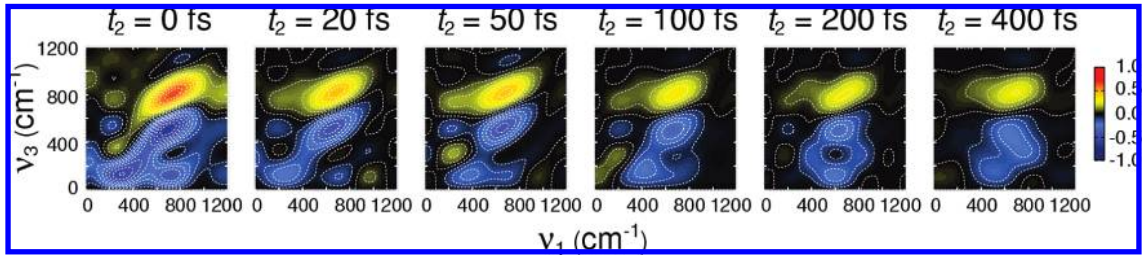

FIGURE 7. 2D IR correlation spectra of liquid water in the absence of the translational motion.

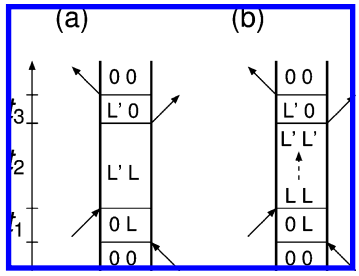

FIGURE 8. Feynman diagrams corresponding to the off-diagonal peak at (~700 cm^{-1}, 150 cm^{-1}). L and L′ denote the excited state of the librational (~700 cm^{-1}) and the low frequency (~150 cm^{-1}) motions, respectively.

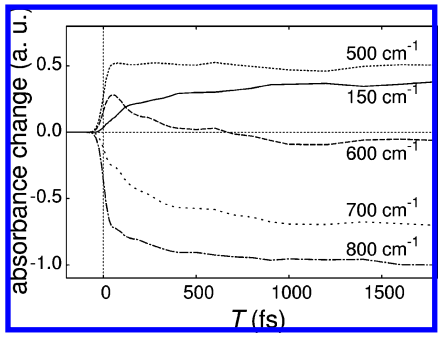

FIGURE 9. Isotropic pump−probe signals for several probe frequencies. The pump frequency is 700 cm^{-1}.

est component of the intensity change of the off-diagonal peak arises from the relaxation to the hot ground state. The intensity change caused by the thermalization is small in Figure 7, because the HB network rearrangement is absent in the translation-free MD simulation.

We can analyze the population relaxation process by using the isotropic pump−probe signal given by

$$\Delta\alpha_{iso}(T) = \frac{\Delta\alpha_{\parallel}(T) + 2\Delta\alpha_{\perp}(T)}{3} \tag{19}$$

where $\Delta\alpha_{\parallel}(T)$ and $\Delta\alpha_{\perp}(T)$ are the absorbance changes of the parallel and perpendicular polarizations, respectively. Figure 9 shows the calculated pump−probe signals for $\omega_{pump} = 700$ cm^{-1} and five different probe frequencies. The absorbance changes for $\omega_{probe} = 700$ and 800 cm^{-1} have the negative peak at $T \sim 0$ fs. This negative peak is attributed to the bleaching and the stimulated emission of the librational motion. The absorbance changes for $\omega_{probe} = 500$ and 600 cm^{-1} have the positive peak at $T \sim 0$

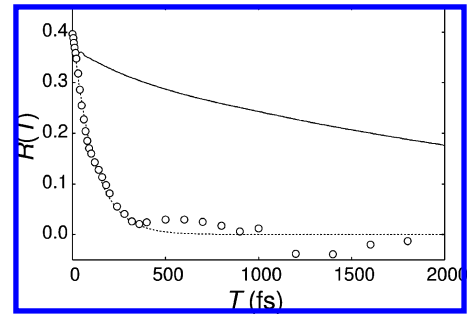

FIGURE 10. Polarization anisotropy decay of the librational motion. Open circles show the anisotropy decay calculated from the third-order nonlinear response function. The dotted line is 0.40 exp(−T/116). The solid line is the orientational correlation function of the total dipole moment.

fs which is attributed to the excited state absorption. The absorbance change for $T > 0$ fs is characterized by two relaxations, i.e. the population relaxation of the librational motion and the relaxation to the hot ground state. The presence of these two relaxations is the most clearly seen in the absorbance change for $\omega_{probe} = 150$ cm^{-1} which does not have any peak at $T \sim 0$ fs. The estimated time scales for the population relaxation of the librational motion and the relaxation to the hot ground state are 60 and 500 fs, respectively. The calculated 2D IR spectra and pump−probe signals clearly reveal the existence of the low frequency (~150 cm^{-1}) intermediate state in the energy relaxation process from the librational motion to the hot ground state.

Woutersen and Bakker found that the anisotropy decay of the OH stretch in pure water is substantially faster than the time scale of the orientational relaxation of a water molecule and concluded that this ultrafast anisotropy decay results from the resonant energy transfer of the OH stretch excitation.[20] The polarization anisotropy is defined as

$$R(T) = \frac{\Delta\alpha_{\parallel}(T) - \Delta\alpha_{\perp}(T)}{\Delta\alpha_{\parallel}(T) + 2\Delta\alpha_{\perp}(T)} \tag{20}$$

Open circles in Figure 10 show the calculated polarization anisotropy of the librational motion. The anisotropy decay is well fit by a single exponential function with a time scale of 116 fs. If the anisotropy decay is caused by the collective orienta-

tional motions, it is expressed by the orientational correlation function of the total dipole moment,

$$C(T) = \frac{2}{5}\left\langle P_2\left(\frac{\mathbf{M}(T)}{|\mathbf{M}(T)|} \cdot \frac{\mathbf{M}(0)}{|\mathbf{M}(0)|}\right)\right\rangle \quad (21)$$

where $P_2(x)$ is the second-order Legendre polynomial. The solid line in Figure 10 is the orientational correlation function of the total dipole moment of the system. The polarization anisotropy decays much faster than the orientational correlation function. This result indicates that once the intramolecular energy is dissipated to the librational motion, the energy of the librational motion quickly transfers to the surrounding molecules through the HB network in water.

V. Conclusions and Outlook

In this Account, we reviewed our recent results on theoretical nonlinear spectroscopies of the intermolecular motions in liquid water. We demonstrated that detailed information about the intermolecular dynamics that is not evident from linear spectroscopies can be elucidated by theoretical nonlinear spectroscopy. 2D Raman spectroscopy shows the large anharmonic coupling between the translational motions and that between the translational and librational motions. The 2D IR spectra, 3PEPS, pump−probe signal, and polarization anisotropy reveal the time scales of the frequency modulation, the population relaxation of the librational motion and the ultrafast intermolecular energy transfer in water. We showed the importance of the HB dynamics in the frequency modulation and the energy relaxation by using the translation-free MD simulation.

We calculated multidimensional spectroscopies by using *ab initio* methods. Multidimensional spectroscopies are expressed by multitime correlation functions. In *ab initio* methods, the multitime correlation function is explicitly evaluated by exploiting the equilibrium dynamics simulation and the nonequilibrium dynamics simulation. *Ab initio* methods are not limited to the intermolecular motions of water. Quantum effects, which are especially important in high frequency intramolecular motion, will be included in *ab initio* methods by introducing an appropriate theory, e.g. linearized semiclassical methods. The idea of the multitime correlation function will provide an efficient tool to investigate the structure and dynamics of interfaces. It will also be available to analyze the slow dynamics of supercooled liquids. Theoretical nonlinear spectroscopy with *ab initio* methods promises to provide important insight into various intramolecular and intermolecular dynamics in condensed phases.

We thank I. Ohmine, K. Ohta, and J. Ono for helpful discussions. The present study was supported by the Grant-in-Aid for Scientific Research on Priority Areas (No. 18066018), the Grant-in Aid for Scientific Research (No. 19350009), the Molecular-Based New Computational Science Program, NINS, and the Next Generation Super Computing Project, Nanoscience program. The calculation has been carried out by using the supercomputers at Research Center for Computational Science in Okazaki.

BIOGRAPHICAL INFORMATION

Takuma Yagasaki obtained his Ph.D. in chemistry from Nagoya University in 2005, working with Iwao Ohmine. He is currently a postdoctoral fellow in the group of Shinji Saito at Institute for Molecular Science. His research interests include theoretical nonlinear spectroscopy of hydrogen bonded liquids and chemical reactions in water.

Shinji Saito received his B.S. in chemistry (1988) from Keio University, his M. Eng. from Kyoto University (1990) and his Ph.D. from the Graduate University for Advanced Studies (1995). He joined the Department of Chemistry at Nagoya University as an assistant professor in 1994 and was promoted to an associate professor in 1998. In 2005, he moved to Institute for Molecular Science as a professor. His research interests include theoretical studies on nonlinear spectroscopy of liquids, slow dynamics of supercooled liquids, and structural fluctuations and chemical reactions in biological systems.

FOOTNOTES

*To whom correspondence should be addressed. E-mail: shinji@ims.ac.jp.

REFERENCES

1 *Water, a Comprehensive Treatise*; Franks, F., Ed.; Plenum: New York, 1972−1982; Vols. 1−7.
2 Eisenberg, D.; Kauzmann, W. *The Structures and Properties of Water*; Oxford: London, 1969.
3 Rahman, A.; Stilling, F. H. Molecular Dynamics Study of Liquid Water. *J. Chem. Phys.* **1971**, *55*, 3336–3359.
4 Stillinger, F. H. Water Revisited. *Science* **1980**, *209*, 451–457.
5 Ohmine, I.; Tanaka, H. Fluctuation, Relaxations, and Hydration in Liquid Water. Hydrogen-Bond Rearrangement Dynamics. *Chem. Rev.* **1993**, *93*, 2545–2566.
6 Ohmine, I.; Saito, S. Water dynamics: Fluctuation, relaxation, and chemical reactions in hydrogen bond network rearrangement. *Acc. Chem. Res.* **1999**, *32*, 741–749.
7 Maroncelli, M.; Macinnis, J.; Fleming, G. R. Polar-Solvent Dynamics and Electron-Transfer Reactions. *Science* **1989**, *243*, 1674–1681.
8 Gertner, B. J.; Whitnell, R. M.; Wilson, K. R.; Hynes, J. T. Activation to the Transition State: Reactant and Solvent Energy Flow for a Model S_N2 Reaction in Water. *J. Am. Chem. Soc.* **1991**, *113*, 74–87.
9 Marx, D.; Tuckerman, M. E.; Hutter, J.; Parrinello, M. The nature of the hydrated excess proton in water. *Nature* **1999**, *397*, 601–604.
10 Lapid, H.; Agmon, N.; Petersen, M. K.; Voth, G. A. A bond-order analysis of the mechanism for hydrated proton mobility in liquid water. *J. Chem. Phys.* **2005**, *122*, 014506.
11 Tuckerman, M. E.; Chandra, A.; Marx, D. Structure and dynamics of OH^-(aq). *Acc. Chem. Res.* **2006**, *39*, 151–158.
12 Lock, A. J.; Bakker, H. J. Temperature dependence of vibrational relaxation in liquid H_2O. *J. Chem. Phys.* **2002**, *117*, 1708–1713.
13 Cowan, M. L.; Bruner, B. D.; Huse, N.; Dwyer, J. R.; Chugh, B.; Nibbering, E. T. J.; Elsaesser, T.; Miller, R. J. D. Ultrafast memory loss and energy redistribution in the hydrogen bond network of liquid H_2O. *Nature* **2005**, *434*, 199–202.

14 Kraemer, D.; Cowan, M. L.; Paarmann, A.; Huse, N.; Nibbering, E. T. J.; Elsaesser, T.; Miller, R. J. D. Temperature dependence of the two-dimensional infrared spectrum of liquid H_2O. *Proc. Natl. Acad. Sci. U.S.A.* **2008**, *105*, 437–442.

15 Huse, N.; Ashihara, S.; Nibbering, E. T. J.; Elsaesser, T. Ultrafast vibrational relaxation of O-H bending and librational excitations in liquid H_2O. *Chem. Phys. Lett.* **2005**, *404*, 389–393.

16 Ashihara, S.; Huse, N.; Espagne, A.; Nibbering, E. T. J.; Elsaesser, T. Vibrational couplings and ultrafast relaxation of the O-H bending mode in liquid H_2O. *Chem. Phys. Lett.* **2006**, *424*, 66–70.

17 Lindner, J.; Vohringer, P.; Pshenichnikov, M. S.; Cringus, D.; Wiersma, D. A.; Mostovoy, M. Vibrational relaxation of pure liquid water. *Chem. Phys. Lett.* **2006**, *421*, 329–333.

18 Lindner, J.; Cringus, D.; Pshenichnikov, M. S.; Vohringer, P. Anharmonic bend-stretch coupling in neat liquid water. *Chem. Phys.* **2007**, *341*, 326–335.

19 Chieffo, L.; Shattuck, J.; Amsden, J. J.; Erramilli, S.; Ziegler, L. D. Ultrafast vibrational relaxation of liquid H_2O following librational combination band excitation. *Chem. Phys.* **2007**, *341*, 71–80.

20 Woutersen, S.; Bakker, H. J. Resonant intermolecular transfer of vibrational energy in liquid water. *Nature* **1999**, *402*, 507–509.

21 Woutersen, S.; Emmerichs, U.; Nienhuys, H. K.; Bakker, H. J. Anomalous temperature dependence of vibrational lifetimes in water and ice. *Phys. Rev. Lett.* **1998**, *81*, 1106–1109.

22 Fecko, C. J.; Loparo, J. J.; Roberts, S. T.; Tokmakoff, A. Local hydrogen bonding dynamics and collective reorganization in water: Ultrafast infrared spectroscopy of HOD/D_2O. *J. Chem. Phys.* **2005**, *122*, 054506.

23 Stenger, J.; Madsen, D.; Hamm, P.; Nibbering, E. T. J.; Elsaesser, T. A photon echo peak shift study of liquid water. *J. Phys. Chem. A* **2002**, *106*, 2341–2350.

24 Fecko, C. J.; Eaves, J. D.; Loparo, J. J.; Tokmakoff, A.; Geissler, P. L. Ultrafast hydrogen-bond dynamics in the infrared spectroscopy of water. *Science* **2003**, *301*, 1698–1702.

25 Eaves, J. D.; Loparo, J. J.; Fecko, C. J.; Roberts, S. T.; Tokmakoff, A.; Geissler, P. L. Hydrogen bonds in liquid water are broken only fleetingly. *Proc. Natl. Acad. Sci. U.S.A.* **2005**, *102*, 13019–13022.

26 Loparo, J. J.; Roberts, S. T.; Tokmakoff, A. Multidimensional infrared spectroscopy of water. I.Vibrational dynamics in two-dimensional IR line shapes. *J. Chem. Phys.* **2006**, *125*, 194521.

27 Loparo, J. J.; Roberts, S. T.; Tokmakoff, A. Multidimensional infrared spectroscopy of water. II. Hydrogen bond switching dynamics. *J. Chem. Phys.* **2006**, *125*, 194522.

28 Asbury, J. B.; Steinel, T.; Stromberg, C.; Corcelli, S. A.; Lawrence, C. P.; Skinner, J. L.; Fayer, M. D. Water dynamics: Vibrational echo correlation spectroscopy and comparison to molecular dynamics simulations. *J. Phys. Chem. A* **2004**, *108*, 1107–1119.

29 Lawrence, C. P.; Skinner, J. L. Vibrational spectroscopy of HOD in liquid D_2O. III. Spectral diffusion, and hydrogen-bonding and rotational dynamics. *J. Chem. Phys.* **2003**, *118*, 264–272.

30 Rey, R.; Moller, K. B.; Hynes, J. T. Ultrafast vibrational population dynamics of water and related systems: A theoretical perspective. *Chem. Rev.* **2004**, *104*, 1915–1928.

31 Moller, K. B.; Rey, R.; Hynes, J. T. Hydrogen bond dynamics in water and ultrafast infrared spectroscopy: A theoretical study. *J. Phys. Chem. A* **2004**, *108*, 1275–1289.

32 Schmidt, J. R.; Corcelli, S. A.; Skinner, J. L. Pronounced non-Condon effects in the ultrafast infrared spectroscopy of water. *J. Chem. Phys.* **2005**, *123*, 044513.

33 Torii, H. Time-domain calculations of the polarized Raman spectra, the transient infrared absorption anisotropy, and the extent of delocalization of the OH stretching mode of liquid water. *J. Phys. Chem. A* **2006**, *110*, 9469–9477.

34 Schmidt, J. R.; Roberts, S. T.; Loparo, J. J.; Tokmakoff, A.; Fayer, M. D.; Skinner, J. L. Are water simulation models consistent with steady-state and ultrafast vibrational spectroscopy experiments? *Chem. Phys.* **2007**, *341*, 143–157.

35 Paarmann, A.; Hayashi, T.; Mukamel, S.; Miller, R. J. D. Probing intermolecular couplings in liquid water with two-dimensional infrared photon echo spectroscopy. *J. Chem. Phys.* **2008**, *128*, 191103.

36 Mallik, B. S.; Semparithi, A.; Chandra, A. Vibrational spectral diffusion and hydrogen bond dynamics in heavy water from first principles. *J. Phys. Chem. A* **2008**, *112*, 5104–5112.

37 Ashihara, S.; Huse, N.; Espagne, A.; Nibbering, E. T. J.; Elsaesser, T. Ultrafast structural dynamics of water induced by dissipation of vibrational energy. *J. Phys. Chem. A* **2007**, *111*, 743–746.

38 Tanimura, Y.; Mukamel, S. 2-Dimensional Femtosecond Vibrational Spectroscopy of Liquids. *J. Chem. Phys.* **1993**, *99*, 9496–9511.

39 Tanimura, Y. Stochastic Lionville, Langevin, Fokker-Planck, and master equation approaches to quantum dissipative systems. *J. Phys. Soc. Jpn.* **2006**, *75*, 082001.

40 Li, Y. L.; Huang, L.; Miller, R. J. D.; Hasegawa, T.; Tanimura, Y. Two-dimensional fifth-order Raman spectroscopy of liquid formamide: Experiment and Theory. *J. Chem. Phys.* **2008**, *128*, 234507.

41 Saito, S.; Ohmine, I. Off-resonant fifth-order nonlinear response of water and CS_2: Analysis based on normal modes. *J. Chem. Phys.* **1998**, *108*, 240–251.

42 Saito, S.; Ohmine, I. Off-resonant fifth-order response function for two-dimensional Raman spectroscopy of liquids CS_2 and H_2O. *Phys. Rev. Lett.* **2002**, *88*, 207401.

43 Saito, S.; Ohmine, I. Fifth-order two-dimensional Raman spectroscopy of liquid water, crystalline ice Ih and amorphous ices: Sensitivity to anharmonic dynamics and local hydrogen bond network structure. *J. Chem. Phys.* **2006**, *125*, 084506.

44 Cho, M.; Fleming, G. R.; Saito, S.; Ohmine, I.; Stratt, R. M. Instantaneous Normal-Mode Analysis of Liquid Water. *J. Chem. Phys.* **1994**, *100*, 6672–6683.

45 Ma, A.; Stratt, R. M. Fifth-order Raman spectrum of an atomic liquid: Simulation and instantaneous-normal-mode calculation. *Phys. Rev. Lett.* **2000**, *85*, 1004–1007.

46 Jansen, T. L. C.; Snijders, J. G.; Duppen, K. The third- and fifth-order nonlinear Raman response of liquid CS_2 calculated using a finite field nonequilibrium molecular dynamics method. *J. Chem. Phys.* **2000**, *113*, 307–311.

47 Denny, R. A.; Reichman, D. R. Mode-coupling theory of the fifth-order Raman spectrum of an atomic liquid. *Phys. Rev. E* **2001**, *6306*, 065101.

48 van Zon, R.; Schofield, J. Mode-coupling theory for multiple-point and multiple-time correlation functions. *Phys. Rev. E* **2001**, *65*, 011106.

49 Kim, J.; Keyes, T. Generalized Langevin equation approach to higher-order classical response: Second-order-response time-resolved Raman experiment in CS_2. *Phys. Rev. E* **2002**, *65*, 061102.

50 Cao, J. S.; Yang, S. L.; Wu, J. L. Calculations of nonlinear spectra of liquid Xe. II. Fifth-order Raman response. *J. Chem. Phys.* **2002**, *116*, 3760–3776.

51 Saito, S.; Ohmine, I. Off-resonant two-dimensional fifth-order Raman spectroscopy of liquid CS_2: Detection of anharmonic dynamics. *J. Chem. Phys.* **2003**, *119*, 9073–9087.

52 Nagata, Y.; Tanimura, Y. Two-dimensional Raman spectra of atomic solids and liquids. *J. Chem. Phys.* **2006**, *124*, 024508.

53 Hasegawa, T.; Tanimura, Y. Calculating fifth-order Raman signals for various molecular liquids by equilibrium and nonequilibrium hybrid molecular dynamics simulation algorithms. *J. Chem. Phys.* **2006**, *125*, 074512.

54 Hasegawa, T.; Tanimura, Y. Nonequilibrium molecular dynamics simulations with a backward-forward trajectories sampling for multidimensional infrared spectroscopy of molecular vibrational modes. *J. Chem. Phys.* **2008**, *128*, 064511.

55 Yagasaki, T.; Saito, S. Ultrafast intermolecular dynamics of liquid water: A theoretical study on two-dimensional infrared spectroscopy. *J. Chem. Phys.* **2008**, *128*, 154521.

56 Mukamel, S. *Nonlinear Optical Spectroscopy*; Oxford; New York, 1995.

57 Cho, M. H. Coherent two-dimensional optical spectroscopy. *Chem. Rev.* **2008**, *108*, 1331–1418.

58 Mukamel, S.; Maddox, J. B. All-forward semiclassical simulations of nonlinear response functions. *J. Chem. Phys.* **2004**, *121*, 36–43.

59 Jansen, T. L. C.; Duppen, K.; Snijders, J. G. Close collisions in the two-dimensional Raman response of liquid carbon disulfide. *Phys. Rev. B* **2003**, *67*, 134206.

60 Hybl, J. D.; Ferro, A. A.; Jonas, D. M. Two-dimensional Fourier transform electronic spectroscopy. *J. Chem. Phys.* **2001**, *115*, 6606–6622.

61 Khalil, M.; Demirdoven, N.; Tokmakoff, A. Obtaining absorptive line shapes in two-dimensional infrared vibrational correlation spectra. *Phys. Rev. Lett.* **2003**, *90*, 047401.

62 Okumura, K.; Tanimura, Y. The (2n+1)th-order off-resonant spectroscopy from the (n+1)th-order anharmonicities of molecular vibrational modes in the condensed phase. *J. Chem. Phys.* **1997**, *106*, 1687–1698.

63 Roberts, S. T.; Loparo, J. J.; Tokmakoff, A. Characterization of spectral diffusion from two-dimensional line shapes. *J. Chem. Phys.* **2006**, *125*, 084502.

64 Joo, T. H.; Jia, Y. W.; Yu, J. Y.; Lang, M. J.; Fleming, G. R. Third-order nonlinear time domain probes of solvation dynamics. *J. Chem. Phys.* **1996**, *104*, 6089–6108.

65 Ohmine, I. Energy-Dissipation Mechanism of the Optically-Excited Molecules in Solvents - a Trajectory Study for a Photoisomerization Process of the Pi-Conjugated Molecule in Ar and Water. *J. Chem. Phys.* **1986**, *85*, 3342–3358.

66 Wilson, K. R.; Levine, R. D. Activated Chemical-Reactions Driven by Accepted Fluctuations. *Chem. Phys. Lett.* **1988**, *152*, 435–441.